

# An investigation of the failure modes in U-10Mo monolithic fuel irradiated to high burnup

March 2023

Charlyne A Smith, Dennis D Keiser Jr, Jan-Fong Jue, Tammy L Trowbridge, Brandon D Miller, Adam B Robinson, Alexander J Winston, Jeffery Giglio





#### DISCLAIMER

This information was prepared as an account of work sponsored by an agency of the U.S. Government. Neither the U.S. Government nor any agency thereof, nor any of their employees, makes any warranty, expressed or implied, or assumes any legal liability or responsibility for the accuracy, completeness, or usefulness, of any information, apparatus, product, or process disclosed, or represents that its use would not infringe privately owned rights. References herein to any specific commercial product, process, or service by trade name, trade mark, manufacturer, or otherwise, does not necessarily constitute or imply its endorsement, recommendation, or favoring by the U.S. Government or any agency thereof. The views and opinions of authors expressed herein do not necessarily state or reflect those of the U.S. Government or any agency thereof.

# An investigation of the failure modes in U-10Mo monolithic fuel irradiated to high burnup

Charlyne A Smith, Dennis D Keiser Jr, Jan-Fong Jue, Tammy L Trowbridge, Brandon D Miller, Adam B Robinson, Alexander J Winston, Jeffery Giglio

March 2023

Idaho National Laboratory Idaho Falls, Idaho 83415

http://www.inl.gov

Prepared for the U.S. Department of Energy Under DOE Idaho Operations Office Contract DE-AC07-05ID14517 An investigation of the failure modes in U-10Mo monolithic fuel irradiated to high burnup

Charlyne Smith<sup>1</sup>, Jan-Fong Jue<sup>1</sup>, Dennis Keiser<sup>1</sup>, Tammy Trowbridge<sup>1</sup>, Brandon Miller<sup>1</sup>, Adam Robinson<sup>1</sup>, Alexander Winston<sup>1</sup>, Jeffery Giglio<sup>1</sup>

Advanced Characterization, Idaho National Laboratory, Idaho Falls, ID 83415, USA

Keywords: U-Mo, high burnup structure, FGP interconnection, crack, blistering

#### Abstract

This study investigated possible failure modes in U-10Mo monolithic fuel irradiated to very-high-burnup. The U-Mo fuel plate used in this study was characterized using scanning electron microscopy, wavelength dispersive spectroscopy, and image analysis techniques to determine how cracks may initiate and propagate through the microstructure. Fission gas pore (FGP) growth was observed near the U-10Mo/Zr interface, and interconnection of the developed pores was observed 5-15 microns away from the U-Mo/Zr interface. The growth, alignment, and interconnection of FGP could initiate blistering of the fuel plate by creating a gas channel for fission gas release along the length of the U-Mo/Zr interface. Due to a grain refinement process that occurs in this fuel at high burnup, the irradiated grain sizes were observed to be at least 20× less than the starting as-fabricated grain size, and the FGP development was most extensive near crack-like defects in the microstructure.

#### 1. Introduction

The United States High Performance Research Reactor (USHPRR) fuel qualification program is qualifying U-Mo fuel for the conversion of high-performance research and test reactors from high-enriched uranium to low-enriched uranium (LEU) [1,2]. U-10Mo monolithic fuel plates are identified as a promising LEU fuel because of their high uranium loading [3,4]; the fuel consists of a uniform U-10Mo foil and Al6061 aluminum cladding. A zirconium (Zr) diffusion barrier was added to the fuel design to minimize the chemical interaction between the U-10Mo and the aluminum alloy cladding [5–7]. Irradiation produces a combination of effects including the generation of fission heat that results in a non-uniform temperature distribution and the accumulation of solid and gaseous fission products in the fuel foil which leads to swelling and a reduction in the fuel's thermal conductivity [8]. Generally, the U-10Mo fuel exhibits stable and predictable irradiation behavior for application in HPRRs; however, nuclear fuels must exhibit an adequate margin to fuel failure during off-normal irradiation conditions [9]. Historically, the

margin to failure has been studied in U-Al dispersion fuels via blister testing [10]. Blisters are formed on the fuel plate when transient conditions-(under-cooled or over-power) result in a rise in temperature exceeding the critical threshold [11]. Studies have investigated the blister-threshold temperature by performing post irradiation heating to discover what temperature results in dimensional instability due to fission gas release [9]. A rise in temperature can result in blister-encouraging effects including (1) stress relaxation in the aluminum cladding due to differential thermal expansion, (2) cladding softening, (3) increased mobility of fission gases, and (4) FGP pressure increase [11]. Blisters are raised regions on the fuel surface that occurs in response to plastic deformation of the aluminum cladding due to large FGP pressure in the fuel meat and/or buckling of the cladding over regions containing damaged fuel [9,11]. The temperature threshold for blistering is conditional to burnup. Continual irradiation results in the degradation of the fuel plate's mechanical properties due to the accumulation of damage, fission products, and pressure in the FGPs. With an increase in the fuel plate temperature, there is a greater thermal expansion in the aluminum cladding than in the fuel meat due to differences in the thermal expansion coefficients [11]. The expansion of the aluminum cladding induces tension into the fuel meat because of the release of the compressive stresses built up in the cladding. Temperature rises can also contribute to slight FGP expansion and could result in the formation of microcracks in the fuel phase [11]. Medvedev et al. proposed that cracking in the U-Mo fuel zone comes from the high porosity and high thermal stresses during reactor shutdown [12]. A comprehensive understanding of the microstructural response during transient events is necessary for understanding U-Mo fuel behavior. To investigate the failure modes in irradiated monolithic U-10Mo fuel at high burnup, this study used electron microscopy techniques and image analysis to characterize a fuel plate that contained high-enriched uranium and was irradiated beyond the fission density that an LEU fuel could achieve  $-6 \times 10^{21}$  fissions/cm<sup>3</sup> [13].

# 2. Material history

The monolithic mini fuel plate, L1P7A0, investigated in this study was irradiated in the advanced test reactor as a part of the Reduced Enrichment Research and Test Reactors (RERTR)-12 campaign. Because one of the goals of the irradiation campaign was to understand blistering behavior in U-Mo fuel beyond the typical burnup threshold for low enriched (<20% U<sup>235</sup>) U-Mo fuel, highly enriched (≥20% U<sup>235</sup>) U-Mo fuel was utilized to achieve very high burnup microstructures. Sample MNT28W was obtained as a cross-section of its parent plate, L1P7A0.

Figure 1 illustrates the cutting diagram showing where the MNT28W cross-section was obtained, and Figure 2(a) shows the surface of the MNT28W cross-section that is examined in this study. The L1P7A0 fuel plate has an average fission density exceeding 100% of the burnup achievable by a low enriched U-Mo. Such a high burnup is accomplished by using 69.6% <sup>235</sup>U in this fuel plate. The fabrication of fuel plate L1P7A0 involved co-rolling a U-10Mo foil and Zr on either side of the foil and then applying the Al6061 cladding via hot isostatic pressing. The L1P7A0 fuel plate was irradiated in the Z3 capsule in the advanced test reactor (ATR) and had an average fission density of  $7.7 \times 10^{21}$  fission/cm<sup>3</sup> and a peak fission density of  $9.25 \times 10^{21}$  fission/cm<sup>3</sup>. Detailed irradiation conditions can be found in Ref [14]. Table 1 summarizes the typical RERTR-12 fabrication conditions, and Table 2 summarizes the irradiation conditions of the monolithic U-Mo fuel investigated in this study.

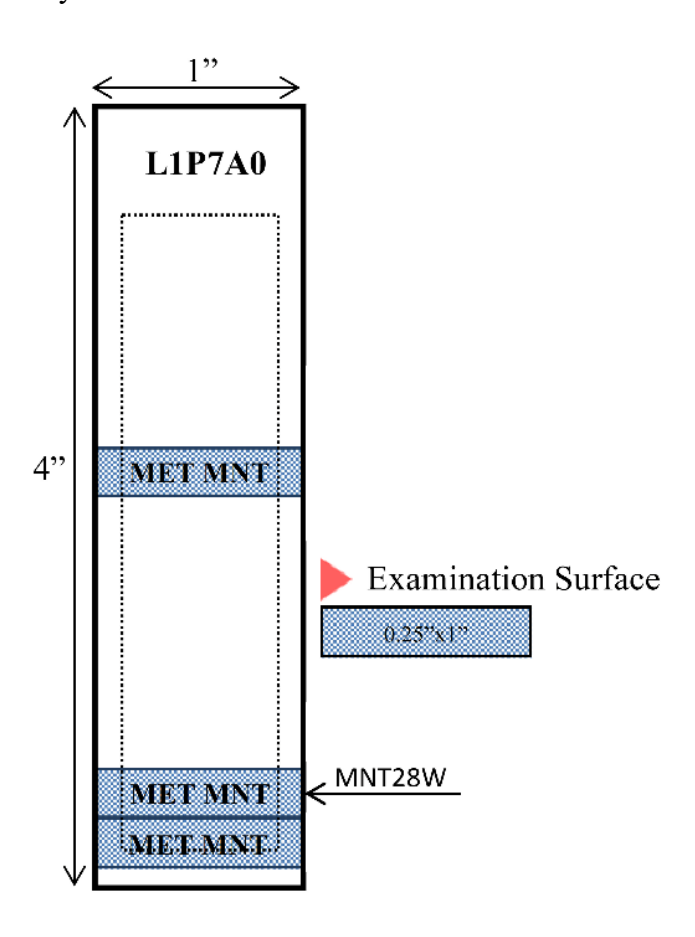


Figure 1. Cutting diagram of L1P7A0 showing where fuel miniplate cross-section MNT28W was obtained.

Table 1. Summary of typical RERTR-12 fabrication conditions.

Fabrication parameters	L1P7A0 (U-10Mo/Zr)	
Feed stock	INL HEU	
Enrichment	69.6%	
Targeted foil thickness,	$300\pm25~\mu m$	
including Zr		
Hot rolling passes	9	
Max hot rolling reduction	40%	
Total hot rolling reduction	85%	
Post hot rolling annealing at	45 min	
650°C		
Cold rolling passes	4	
Total cold rolling reduction	20%	
Total time at 60°C	125 min	
HIP run temperature	560 °C	
HIP run pressure	103 MPa	
HIP bonding time at 560°C	90 min	
HIP run variables	Six plates per HIP can	

Table 2. Summary of irradiation conditions.

Irradiation conditions	L1P7A0 (U-10Mo/Zr)		
Fission power density	12720.43 W/cm <sup>3</sup>		
Fission Heat Rate	882.41 W/g		
Fission Density (averaged)	7.71×10 <sup>21</sup> fissions/cm <sup>3</sup>		
Capsule Cumulative	137.2		
<b>Effective Full Power Days</b>			

# 3. Experiment

Optical microscopy was used to image the MNT28W complete fuel cross-section. Four large-area lift-outs (LALOs) were cut from the MNT28W fuel cross-section using the plasma focused ion beam (PFIB) instrument located in the Irradiated Materials Characterization Laboratory (IMCL) at Idaho National Laboratory (INL). The PFIB was used to create LALOs representative of specific microstructures for chemical and physical characterization of the fuel cross-section, unperturbed by mechanical polishing. The process of preparation of the LALOs is similar to that of a transmission electron microscopy (TEM) sample or lamella [15]. However, the surface area of the LALOs is larger than that of a TEM lamella, averaging 25μm × 22μm × 4μm in this work compared to a typical TEM lamella of  $20\mu m \times 10\mu m \times 100nm$  [15]. The scanning electron microscope (SEM) equipped with wavelength dispersive spectroscopy (WDS) capability was used to obtain back scattered electron (BSE) micrographs, secondary electron micrographs and chemical composition maps. SEM imaging and analysis provides insight into the development of FGPs in the microstructure as well as the distribution and behavior of fission products in the fuel matrix. The FGPs were characterized using the FGP graphical user interface (FGP-GUI) image processing [16,17]. The FGP-GUI uses a series of image processing functions to isolate and segment the FGPs in irradiated U-Mo specimens. To reduce the noise in the micrographs, the FGP-GUI first uses the bilateral filter function to replace each pixel intensity with a weighted average of the intensity of the neighboring pixels. Subsequently, sauvola thresholding is employed to perform FGP segmentation by defining a threshold for each pixel to generate a binary image based on stable variable contrast regions. After sauvola segmentation, the despeckle function removes small clusters of pixels in the binary output prior to filling partially segmented FGP features. Lastly, the border pixel function clears FGP features that are in direct contact with the micrograph borders to eliminate partial or cut off FGPs during acquisition.

#### 4. Results and discussion

# 4.1 Microscopy

Optical microscopy was performed to provide an overview of the transverse cross-section of the fuel plate; the individual optical micrographs were stitched to create Figure 2. Figure 2(a,b) reveals an extended crack along the transverse length of the fuel plate near the U-Mo/Zr interface.

The initiation and growth of cracks is suggestive of interconnection of porosity and fission gas release in the fuel region. However, the brittle nature of the irradiated microstructure combined with compressive stresses in the fuel meat released during cross-section preparation may also contribute to cracking observed in the fuel microstructure. Although de-bonding/crack formation is observed near the Zr diffusion barrier, the cladding was not breached. There are two features associated with de-bond formation in Figure 2(a): (1) the existence of large cracks/pores, mainly parallel to the U-Mo/Zr interface, and (2) plastic deformation of U-Mo fuel meat. The crack parallel to the U-Mo/Zr interface extended through most of the width of the fuel zone and terminated at the plate edge.

The crack in Figure 2(b) is ~100 microns wide and >10mm long. The presence of the crack may explain abnormal swelling behavior observed in the fuel plate. The Helios PFIB SEM was used to create ~24μm ×15μmLALOs to investigate the fuel microstructure in two main regions: region A and region B illustrated in Figure 2(c). LALO A1 was obtained within 2mm of the fuel edge in region A which means that A1 represents the microstructure at the plate edge where there appears to be some swelling restriction. A1 was obtained such that the U-Mo fuel phase and the U-Mo/Zr interface were captured. Three additional LALOs were extracted from region B: (1) B1 captures U-Mo fuel phase and U-Mo/Zr interface, (2) B2 captures U-Mo fuel phase, and (3) B3 captures U-Mo fuel microstructure within 5μm of the crack.

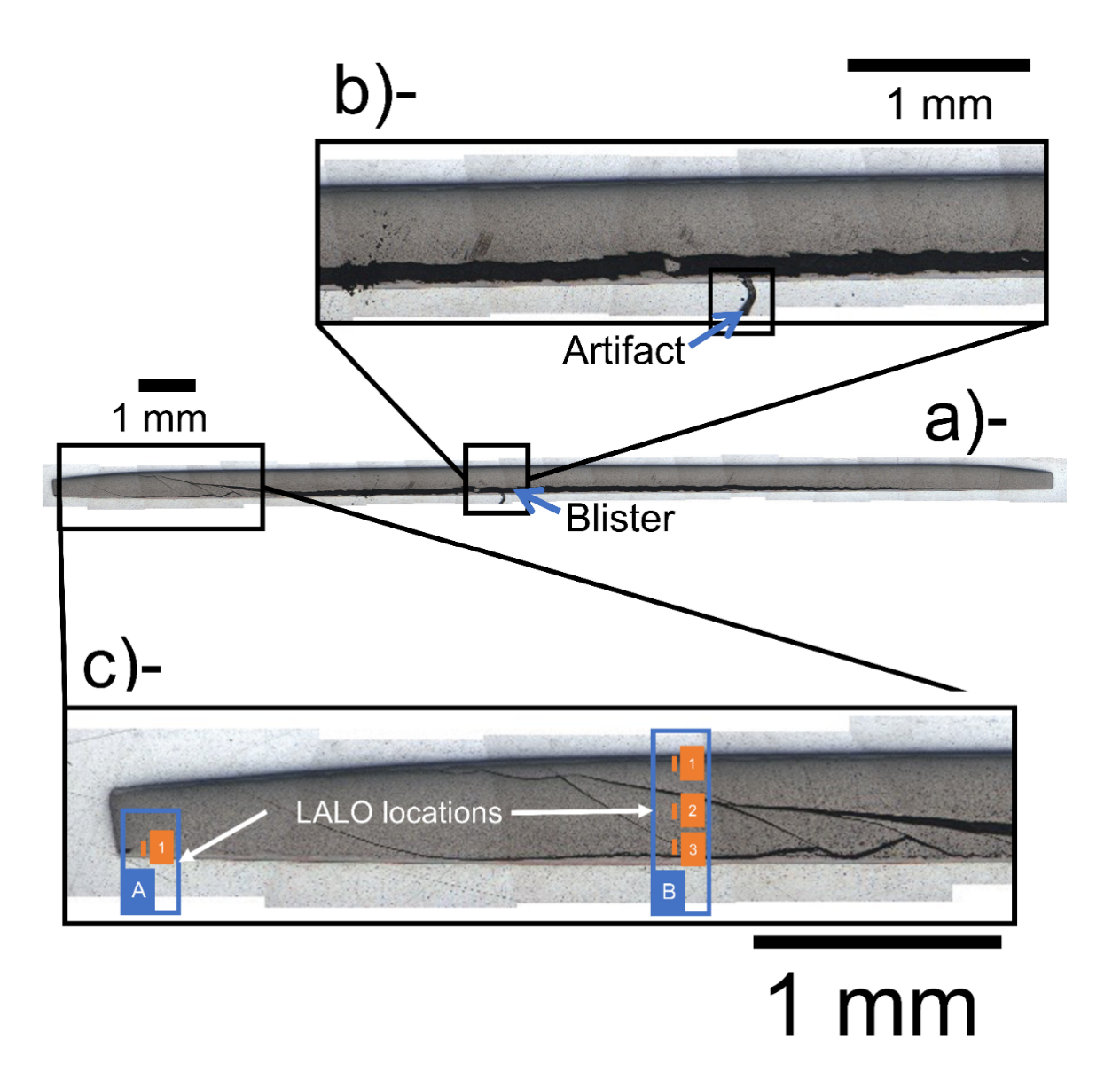


Figure 2. Stitched optical micrographs showing an (a) overview of the fuel miniplate, (b) crack along the transverse cross-section, and (c) regions where LALOs were obtained for SEM and WDS analysis.

Figure 3 highlights the four LALOs using BSE micrographs representative of the microstructures from A1, B1, B2, and B3. The BSE micrographs allow visual assessment of the microstructure where refined U-Mo grains can be seen inside the FGPs in Figure 3. The refined grains have undergone grain subdivision from the original as-fabricated size between 5µm and 10µm and is further discussed in the high burnup structure section. Recall that A1 was extracted near the fuel plate edge where swelling appears restricted likely due to constrain from the cladding [11]. Sample A1 reveals the microstructure of the interface between the U-Mo fuel phase and the Zr diffusion barrier such that there is some diffusion of the Zr into the fuel,

possibly caused by the compression of the cladding rails during neutron irradiation. Prior to irradiation, the U-Mo/Zr interface consists of three major sub-layers: UZr<sub>2</sub>, Mo<sub>2</sub>Zr, and U with low Mo [18]. During irradiation, the UZr<sub>2</sub> sub-layer remains stable without the accumulation of large porosity; however, with increasing burnup, the UZr<sub>2</sub> sub-layer becomes increasingly discontinuous [18]. On the other hand, the low Mo sub-layer exhibits high porosity at low burnup. At higher burnups, the low Mo sub-layer develops large interconnected porosity at least 5μm away from the original location of the sub-layer [18].

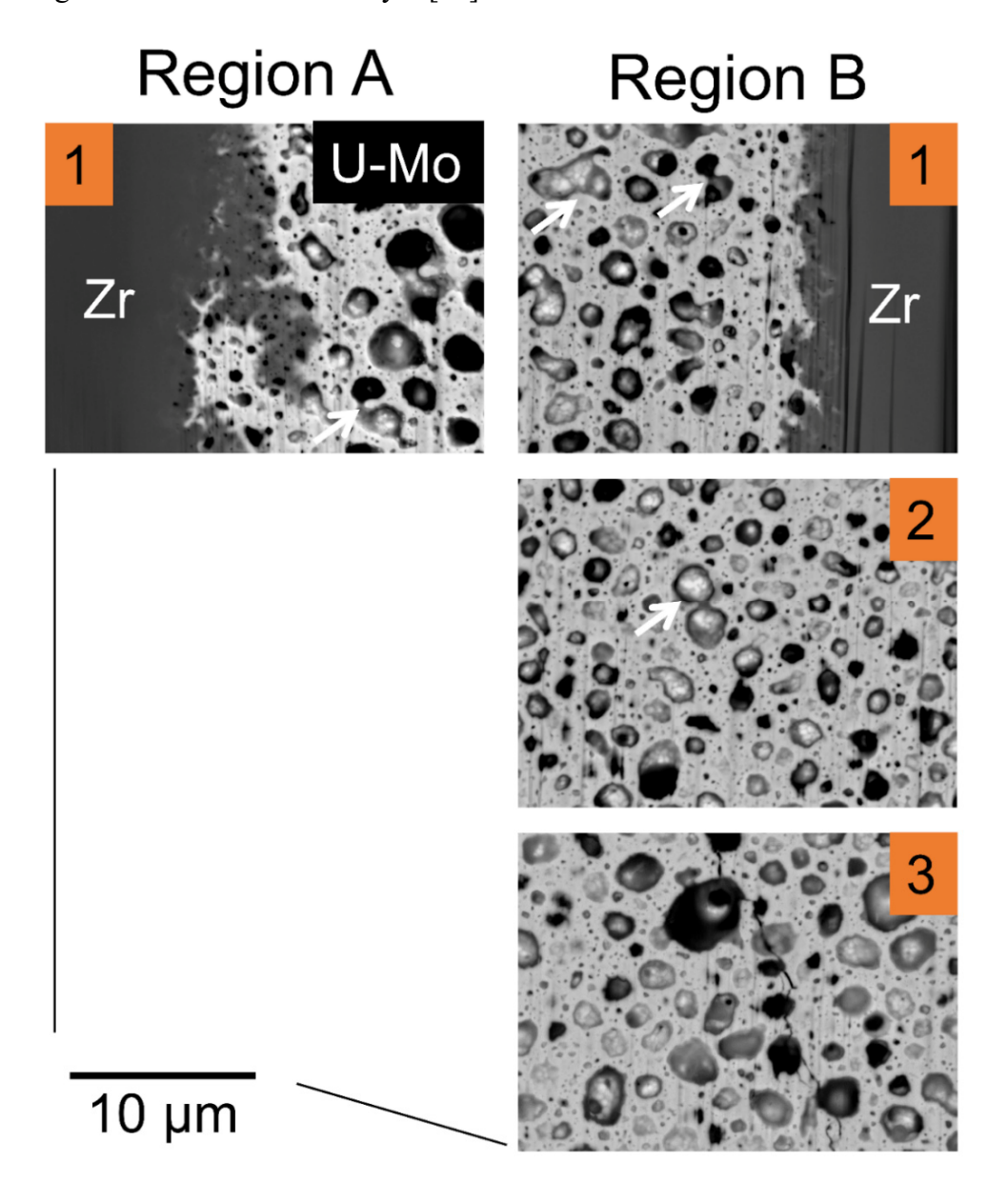


Figure 3. BSE micrographs showing the microstructure of (a) the fuel phase in region B and the U-Mo/Zr interface at region A. Arrows show interconnected pores.

The fuel microstructure in A1 shows the distribution of nm-sized up to  $\mu$ m-sized FGPs where the larger  $\mu$ m-sized pores are seemingly parallel approximately 5-10 $\mu$ m from the Zr barrier. Similarly, sample B1 was extracted to assess the interface between the U-Mo phase and the Zr diffusion barrier, with the exception that sample B1 was taken >2mm away from the fuel plate edge. Based on the BSE micrograph provided in Figure 3 on B1, there was interdiffusion of U, Mo, and Zr; however, interdiffusion of U, Mo, and Zr is not as extensive as observed in A1.

Like sample A1, an alignment of larger FGPs is observed 5-10 μm away from the Zr diffusion barrier in B1. Further, there is evidence of FGP interconnection shown by the white arrows in Figure 3. The alignment and interconnection of the FGPs near the U-Mo/Zr interface could have been a pre-cursor to the formation of the 100μm-wide crack that extends along the transverse cross-section of the plate between the U-Mo phase and the Zr diffusion barrier in Figure 2. Interestingly, FGP interconnection is also observed in sample B2; however, it is observed to a lesser extent in comparison to sample B1. The alignment of FGPs near the U-Mo/Zr interface in B1 was further investigated using the secondary electron (SE) micrograph in Figure 4. Continued preferential alignment of larger FGP structures parallel to the Zr diffusion barrier was observed up to 15 μm away from the Zr barrier.

Finally, the microstructure of sample B3 is also interesting because the sample was obtained within 5µm of the crack extension in the parent fuel plate. As such, the proximity to the crack allowed some propagation in sample B3. Figure 5 shows a BSE micrograph of sample B3 revealing the micro-crack trails interconnected via FGPs indicated by white arrows. Like B2, sample B1 was obtained from the U-Mo fuel phase and reveals the behavior and morphology of the FGPs. Sample B3 in Figure 3 reveals the propagation of a small crack through the microstructure such that the crack infiltrates the FGP periphery. It is also important to note that the FGPs do not seem to be interconnected, which suggests that crack propagation can occur without FGP interconnection in the fuel phase. Based on the microstructures presented in Figure 3, it is believed that interconnection and alignment of FGPs near the U-Mo/Zr interface is the precursor for crack formation in U-Mo.

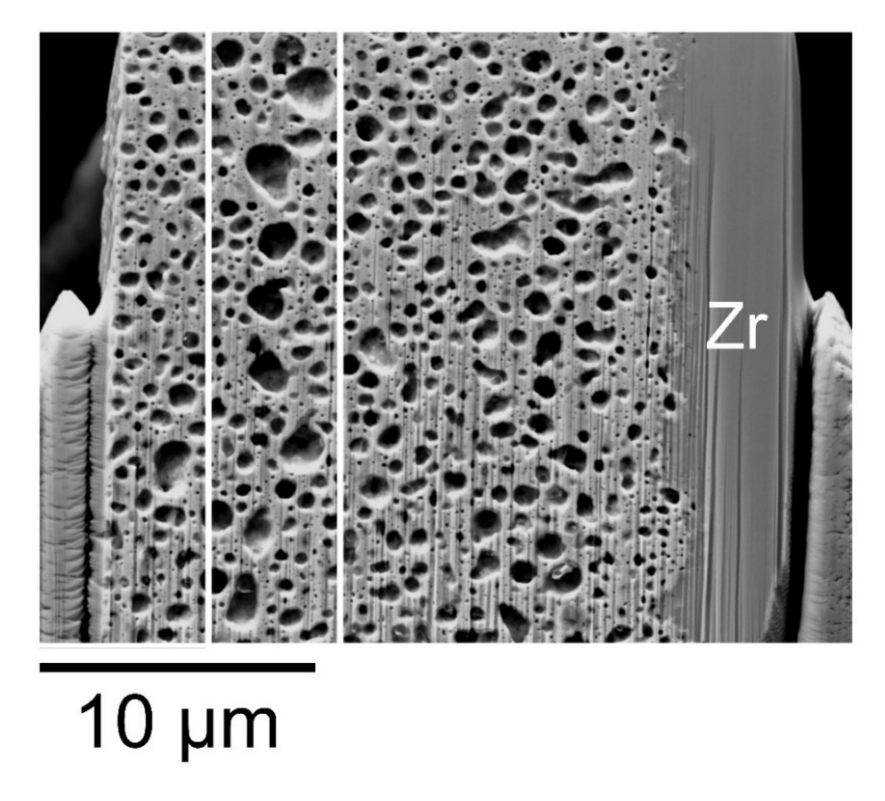


Figure 4. SE micrograph illustrating the preferential alignment of large FGP structures parallel to the Zr diffusion barrier in sample B1.

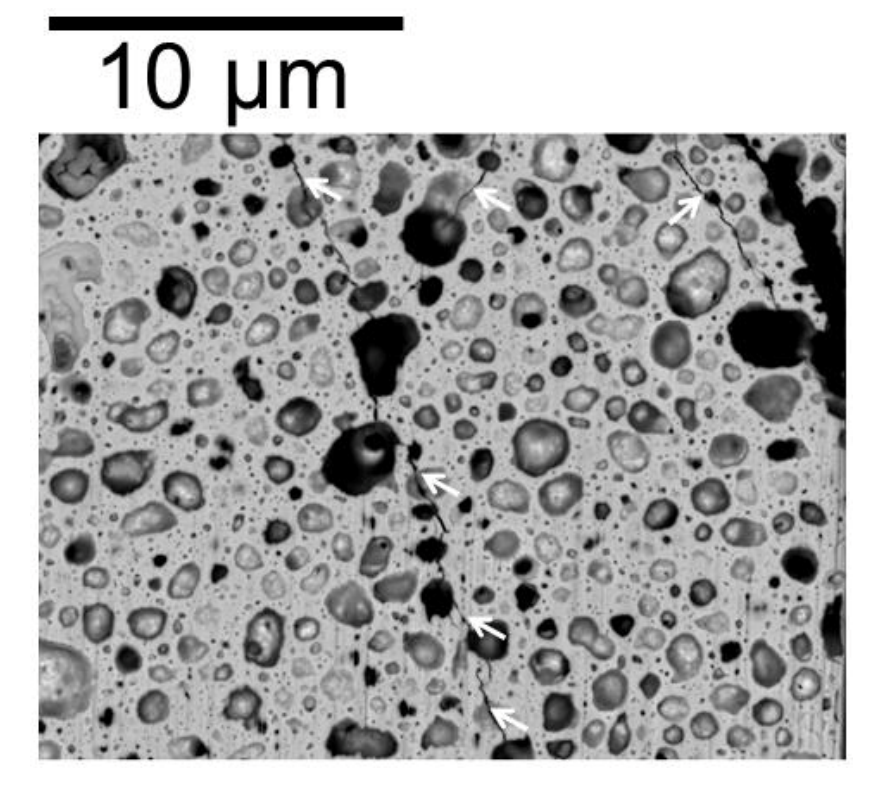


Figure 5. BSE micrograph illustrating micro-cracks through the FGPs in B3.

# 4.2 High burnup structure

The four LALOs in this study exhibited high burnup structure (HBS). HBS describes the result of the restructuring process during irradiation to high burnup. The HBS is characterized by the redistribution of fission gases and extended defects, as well as grain subdivision [19]. Prior to irradiation, the starting grain size ranged from 5–10 µm [5]; however, after irradiation, the grain sizes were reduced to range from 0.2-0.5 µm. Studies have shown that polygonization – the arrangement of dislocations into dislocation walls that form small energy and low-angle grain boundaries (LAGBs) (with < 15 ° misorientation) with slightly misoriented subgrains between the low angle dislocation walls – leads the restructuring process [19,20]. However, recent studies theorize that dynamic recrystallization is also an active mechanism and that polygonization and dynamic recrystallization occur in tandem [19]. Figure 6 reiterated the overview from which the LALO sample A1 and B1 were extracted using the optical micrograph provided in Figure 2(c) in addition to BSE micrographs acquired at high resolution. A closer look at the LALOs extracted near the U-Mo/Zr interface in Figure 6 shows what appears to be grain boundaries indicated by the blue arrows. It is difficult to visually distinguish between the FGP sizes of A1 and B1.

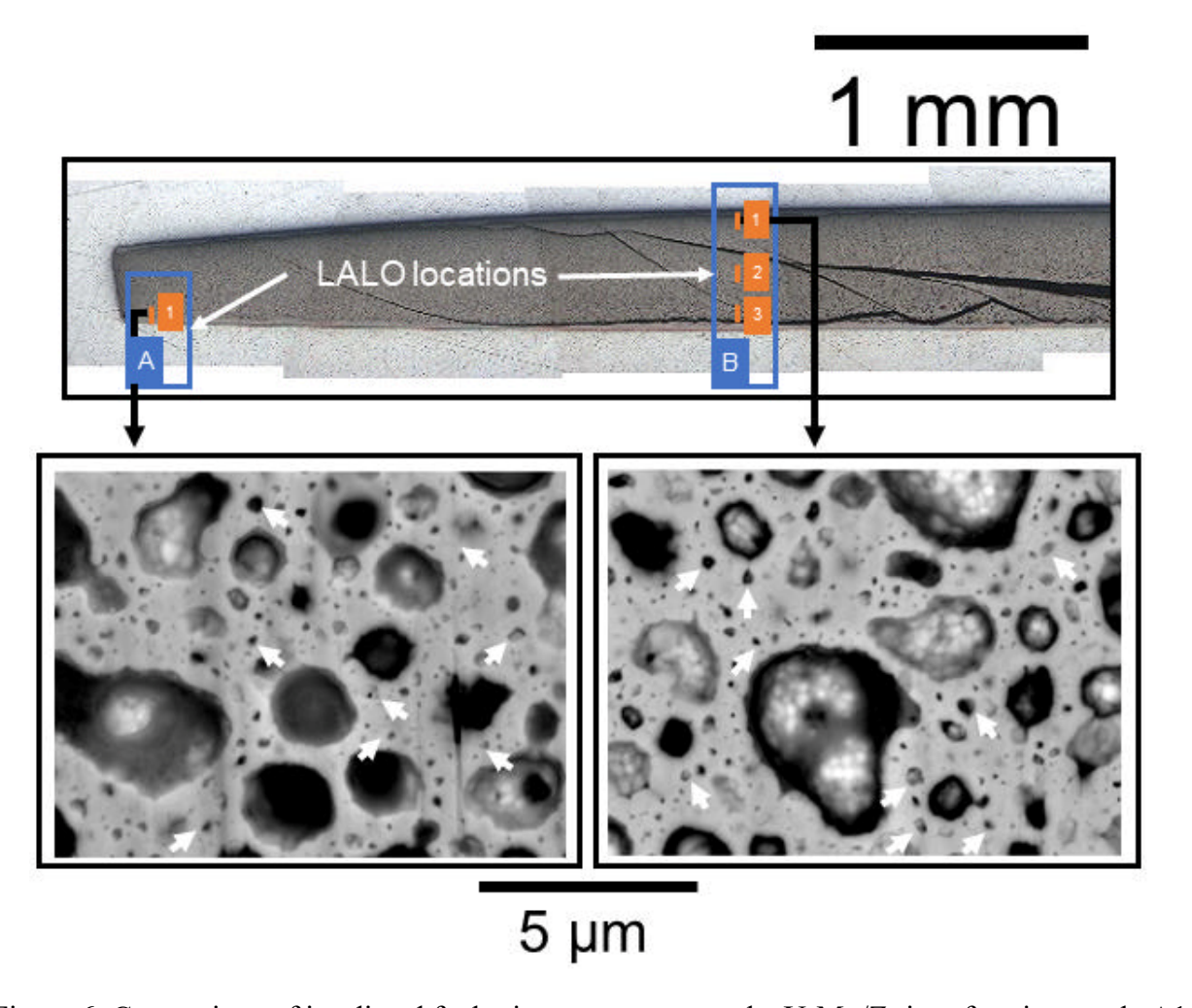


Figure 6. Comparison of irradiated fuel microstructure near the U-Mo/Zr interface in sample A1 and sample B1 with arrows pointing to the intersection of multiple refined grain boundaries.

The BSE micrograph in Figure 6 shows the inclusion of structures, presumably refined U-Mo grains due to the lighter contrast, which is an indicator of a high atomic number in BSE analysis within the FGPs. Further, a halo structure around the FGP periphery is observed. The irradiated grain sizes were at least 20× less than the starting as-fabricated grain size. The FGPs are visually larger than the refined grains; however, there exists smaller FGPs that accumulate along the refined grain boundaries and at triple junctions. FGP growth is evidently favored at the triple junctions while the finer FGPs align along the refined grain boundaries.

The LALOs extracted in the U-Mo fuel phase were also investigated at a higher resolution in Figure 7. Figure 7 reiterated the overview from which the LALO B2 and B3 were extracted using the optical micrograph provided in Figure 2(c) in addition to BSE micrographs acquired at

high resolution. The HBS of B2 and B3 is not significantly different from that of A1 and B1. One of the first observations was the FGP size difference between B2 and B3, where B2 exhibited smaller FGP sizes compared to B3.

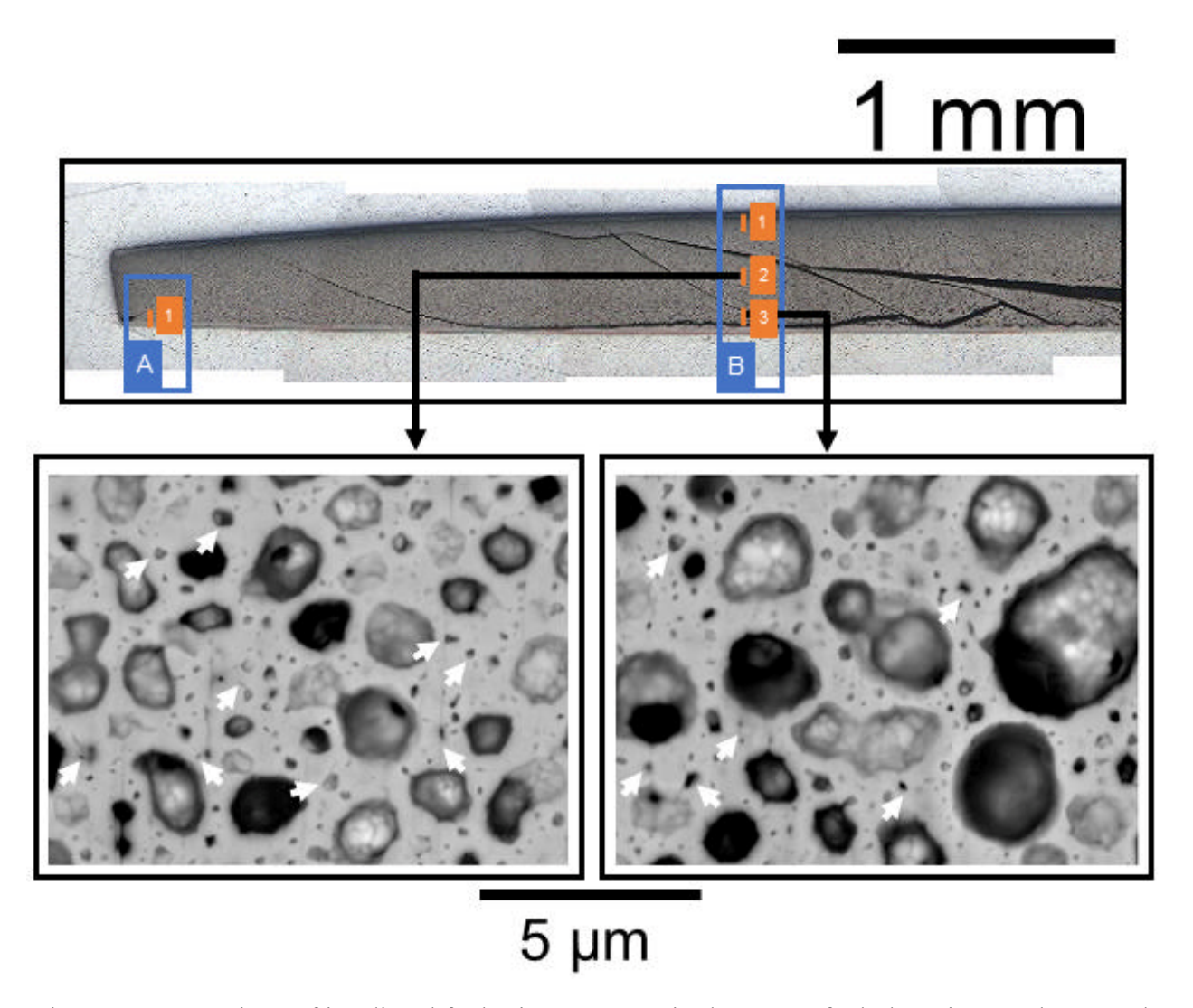


Figure 7. Comparison of irradiated fuel microstructure in the U-Mo fuel phase in sample B2 and sample B3 with arrows pointing to the intersection of multiple refined grain boundaries.

The location where the LALOs were obtained could explain the discrepancy in FGP size between B2 and B3. B3 was extracted within 5µm of the crack near the bottom lane of the fuel plate while B2 was extracted approximately 50µm away from the nearest crack. Damage and fission gas accumulation is higher in B3 due to its proximity to the extended crack, which is believed to contribute to FGP expansion observed in B3. The refined structures observed in A1 and B1 are also present in B2 and B3 and will be discussed in the chemical analysis results. The refined grain

boundaries are highlighted in Figure 7 for B2 and B3. The same behavior at A1 and B1 is documented in B2 and B3 where finer FGPs align along the refined grain boundaries while larger FGPs are found at triple junctions. FGP growth is observed to be accelerated at triple junctions.

#### 4.3 Fission gas pore morphology

The morphology of the FGPs in the four samples is more clearly summarized using the BSE micrographs in Figure 8. The first row provides micrographs of the FGP microstructure in A1, the second row shows B1 FGP microstructure, the third row shows B2, and the final row shows B3. The FGP morphology was quantitatively assessed using the FGP-GUI [21]. Table 3 summaries the FGP morphology including the porosity, area, diameter, and eccentricity. Sample A1 possessed the lowest porosity and FGP size of all four LALOs, presumably because A1 was extracted from the fuel plate edge within 2mm of the fuel plate edge. Swelling at the plate edge is believed to be counteracted by the compressive stresses of the cladding rails that held the fuel plate in place during neutron irradiation. On the other hand, the porosity of the LALOs in region B were very similar averaging at 34.78%. Interestingly, although the porosity among B1, B2, and B3 is similar, the FGP size varies distinctly. The largest FGP sizes were observed in B3, likely because B3 was extracted from within 5µm of the crack shown in Figure 2(c). The second largest FGP sizes were observed in B1 near the U-Mo/Zr interface. The alignment of large porosity near the U-Mo/Zr interface as shown in Figure 4, is a contributor of the FGP size in B1. Of the LALOs extracted from region B, sample B2 exhibited the smallest FGP size. B2 was retrieved from the U-Mo fuel phase ~50 μm from the nearest crack. The influence of eccentricity appears insignificant as the four LALOs investigated in this study is consistently 0.6.

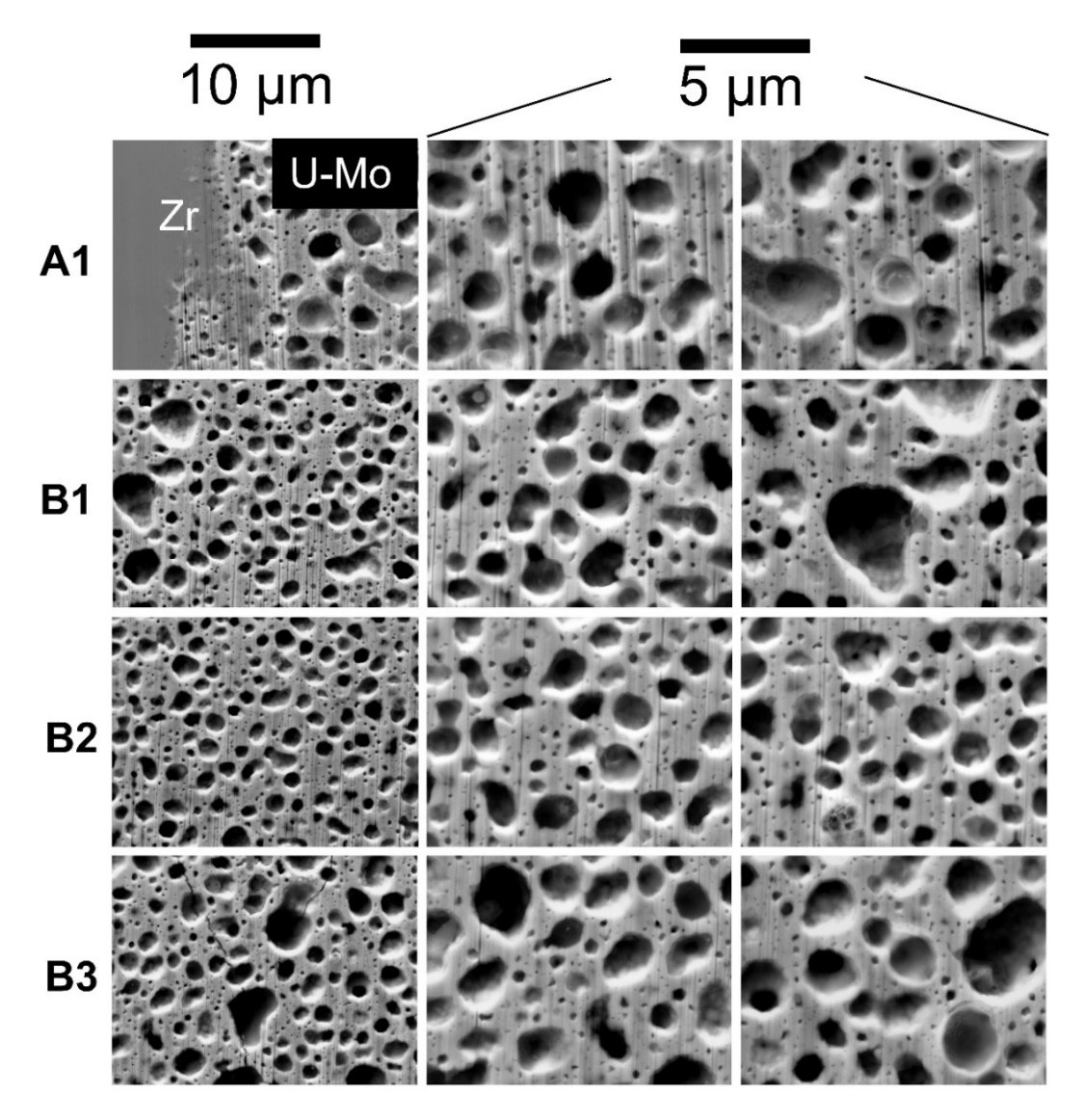


Figure 8. FGP microstructure in A1, B1, B2 and B3. The first, second, third and fourth row correspond to samples A1, B1, B2, and B3 respectively.

Table 3. FGP morphology summary.

Mean parameters	A1	B1	B2	В3
FGP porosity (%)	27	34.7	34.6	34.8
FGP area (µm²)	0.30	0.38	0.34	0.45
FGP diameter (μm)	0.43	0.52	0.52	0.6
FGP eccentricity	0.62	0.60	0.62	0.60

# 4.4 Chemical composition

The elemental distribution of the fission products and some impurities in samples A1, B1, B2 and B3 were assessed using WDS characterization. The crack extended for most of the transverse length of the fuel plate but, eventually, reduced in thickness and came to a halt as it approached the fuel plate edge. It was of interest to assess the fission product behavior at the plate edge, i.e., sample A1. Figure 9 reiterates the microstructure of A1 in addition to the associated WDS chemical maps which highlights fission product behavior. The WDS map for sample A1 in Figure 9 investigated the distribution of oxygen (O), iron (Fe), strontium (Sr), zirconium (Zr), molybdenum (Mo), tellurium, xenon (Xe), cesium (Cs), barium (Ba), cerium (Ce), neodymium (Nd) and uranium (U).

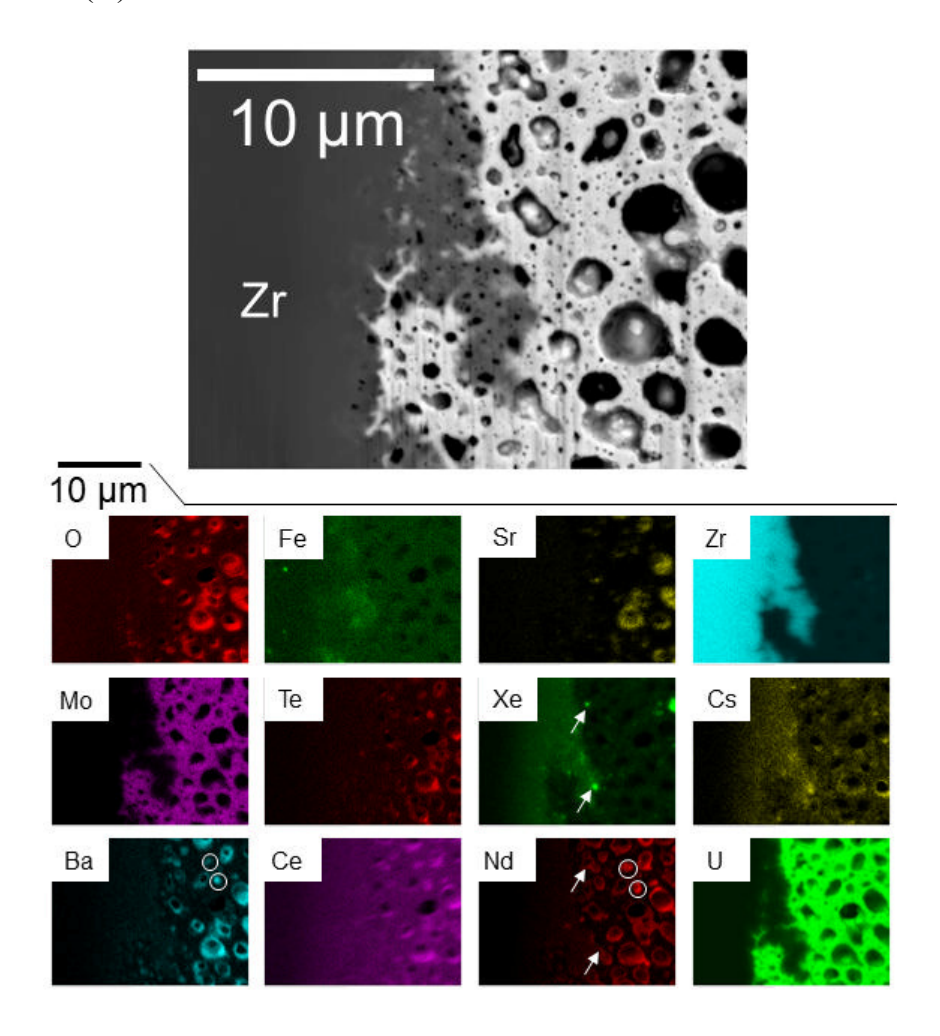


Figure 9. BSE micrographs and WDS chemical maps of sample A1

Figure 9 shows that most of the fission products appear to remain in the U-Mo fuel phase in A1 except for Xe and Cs. Although Sr, Te, Ba, and Nd exclusively remain in the U-Mo fuel phase, their interaction within the fuel phase is such that they overlap. For example, Ba and some Xe is seemingly coated or trapped by Nd because there is some overlap in WDS signals for Ba, Xe and Nd. Studies suggest that > 4at.% Xe it can get trapped in solid fission product inclusions in the fuel matrix [4]. It is possible that Xe precipitates in Figure 9 are trapped inside an enclosed bubble or a solid fission product inclusion near the section surface. On the other hand, Cs can be found in both the Zr diffusion barrier and the U-Mo fuel phase. Xe and Cs penetrated the Zr diffusion at least 4μm in A1. The penetration of the fission products like Xe and Cs into the Zr barrier could be because of irradiation-enhanced diffusion or recoil. Nonetheless, the thickness of the Zr barrier is adequate for limiting fission product penetration. Figure 9 confirms the interdiffusion of U, Mo, and Zr. O is an impurity that appears to have an affinity to the fission products in the U-Mo fuel phase. It is important to note that Fe is an intrinsic impurity in both Zr and Mo, which explains why Fe impurities were observed both in the U-Mo fuel phase and the Zr barrier.

Like sample A1, B1 was obtained at the U-Mo/Zr interface, with the exception that B1 was away from the fuel plate edge. Recall that FGP alignment and interconnection were observed parallel to the U-Mo/Zr interface. Figure 10 shows the WDS chemical maps taken from sample B1. Nd, Cs, and Xe showed the strongest fission product signals in B1. The distribution of fission products in sample B1 is like that observed at the U-Mo/Zr interface in sample A1. Xe is trapped in the Zr diffusion barrier likely from recoils and diffusion. Xe gas penetrated within 4µm of the Zr diffusion barrier in B1. It is known that most of the Xe produced is kept in the fuel matrix; however, it is a challenge to detect the Xe in WDS when the microstructure is high in porosity. The Xe being detected are those which are likely enclosed in a bubble structure or solid fission product inclusion very close to the focused ion beam (FIB)-sectioned surface but not directly intersected with the surface. Nd exhibited the fission product highest concentration in the U-Mo fuel phase at the FGP sites. Fe enrichment is observed at the U-Mo/Zr interface; however, the influence of Fe on microstructural degradation appears to be trivial.

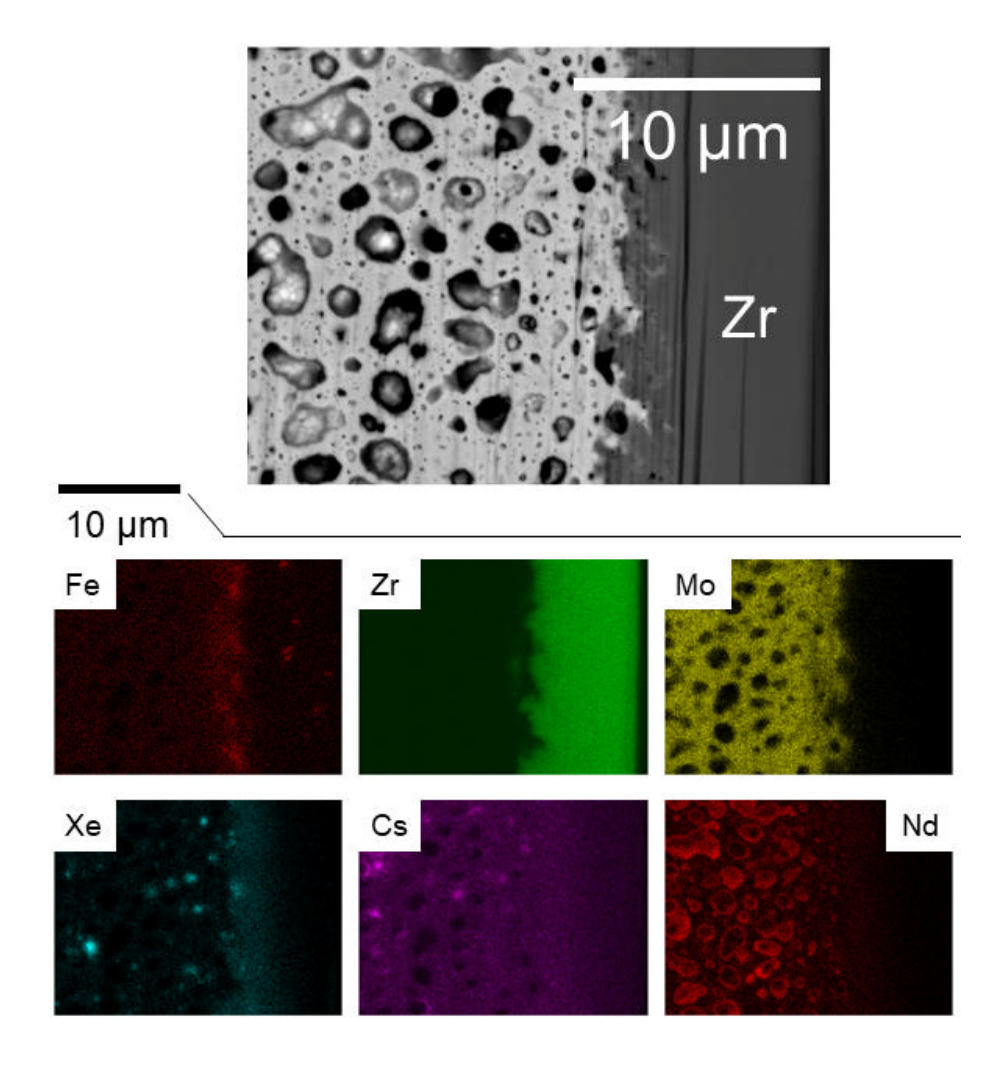


Figure 10. BSE micrographs and WDS chemical maps of sample B1.

Sample B2 captures the U-Mo fuel phase microstructure away from the U-Mo/Zr interface. FGP interconnection is evident in B2; however, it is less dramatic than the FGP microstructure at the U-Mo/Zr interface in B1. Figure 11 provides the WDS chemical maps showing the compositional distribution in B2. As shown in the WDS map, of the detected fission products, Nd chemical signal was highest in the U-Mo fuel phase. Xe and Cs are less concentrated and faintly distributed in the U-Mo fuel phase compared to Nd. The low concentration of Xe and Cs in the fuel phase is likely due to fission gas released during FIB preparation. The segregated signals observed are possibly due to the enclosure of the fission products in a bubble defect or solid fission product inclusion. Figure 11 also shows evidence of Mo chemical banding and diffuse

low-concentration Zr in the fuel matrix. The periphery of the FGPs in the fuel phase appears to be oxidized.

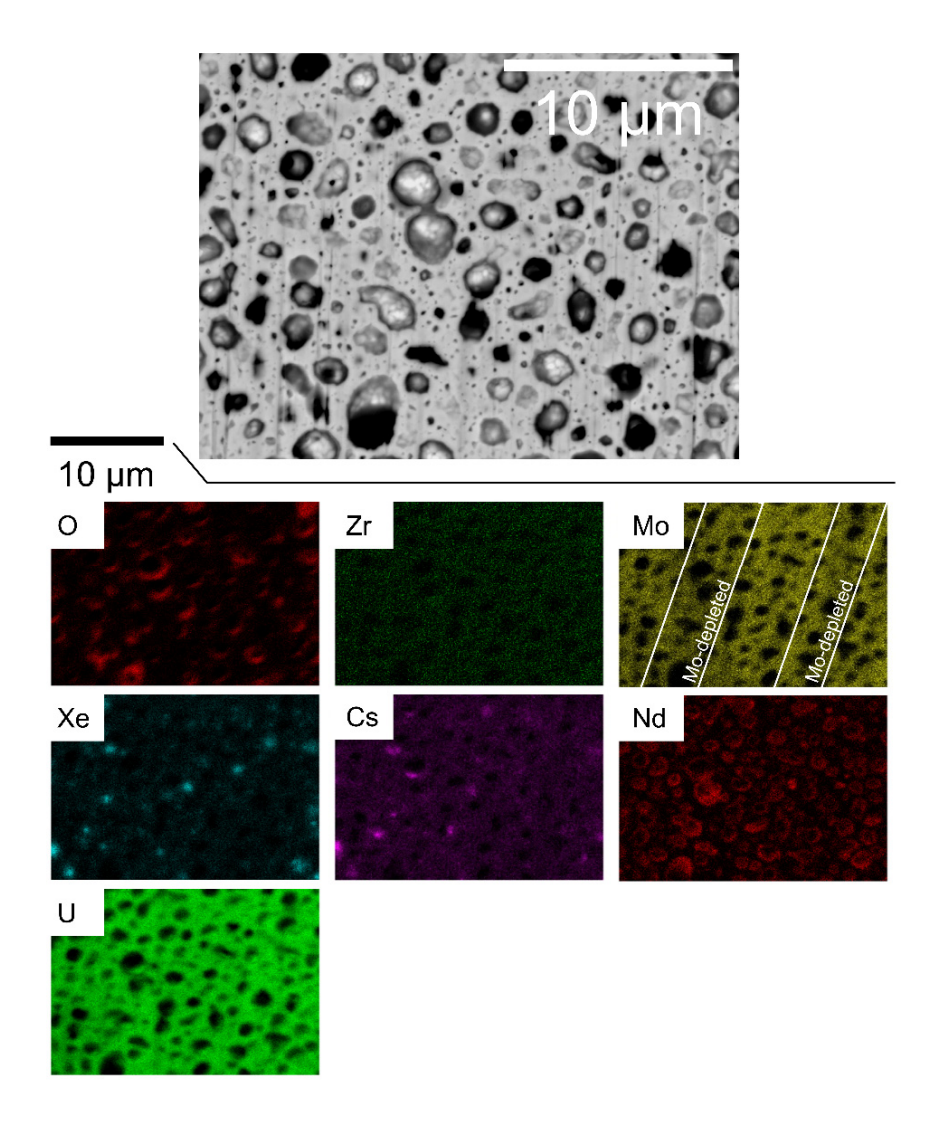


Figure 11. BSE micrographs and WDS chemical maps of sample B2.

Like sample B2, sample B3 depicts the microstructure of the U-Mo fuel phase; however, B3 was obtained within 5µm of the crack shown in Figure 2(c). The crack propagates through the microstructure via the existing FGPs facilitating the release of fission gases. The compositional distribution in B3 is shown in Figure 12 where phases enriched in Ba, La, Ce, and Pr can be observed. The Xe chemical map is like that seen in B1 where the segregated signals are enclosed

possibly by a bubble defect, the majority of the Xe likely escaped during LALO preparation using the FIB. The larger  $100\mu m$ -wide crack that spans most of the transverse length of the fuel creates a network of smaller micro-cracks into the fuel midplane. The results showed that large, interconnected fission gas porosity can align between 5-15 $\mu m$  away from the U-Mo/Zr interface, thereby creating a pathway for cracking to occur in the fuel phase. Phases observed near the U-10Mo interface with the Zr diffusion barrier include: UZr<sub>2</sub>,  $\gamma$ -UZr, Zr solid solution and Mo<sub>2</sub>Zr phases. Small amounts of  $\alpha$ -U were also observed in the Mo depleted zone that forms [13]. The integrity of the U-Mo/Zr remained intact and was not the identified site for crack initiation in monolithic U-Mo fuel.

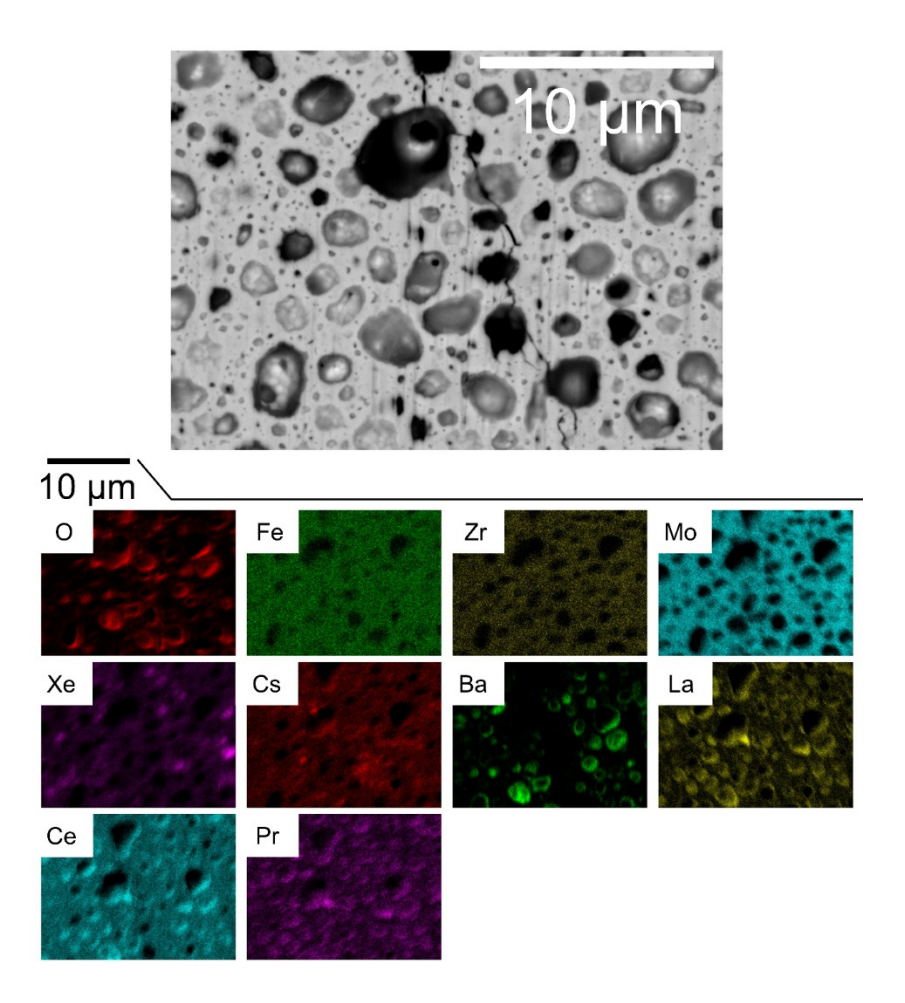


Figure 12. BSE micrographs and WDS chemical maps of sample B3.

The temperature and stress buildup are highest at and in the vicinity of the large crack, as demonstrated by the reduction in FGP size with increasing distance away from the plane of the crack. Based on a previous PIE study of other monolithic fuel plates [18], the pre-irradiation microstructure at the U-Mo/Zr interface seems to recrystallize later than the bulk of the U-Mo fuel meat. In this study, only small, sub-micron bubbles were observed in this interfacial area. The stress, fission density, and temperature at the U-Mo/Zr interface, together with the interdiffusion of U, Mo, Zr and fission products, will need to be properly understood to explain such behavior. No detailed information on the thickness evolution (swelling profile) is currently available. As such, further studies on FGP behavior and other factors that could influence crack/void formation in the fuel meat are needed.

#### 5. Conclusion

Electron microscopy and image analysis were used to investigate the potential failure modes in U-10Mo monolithic fuel plates irradiated to a very high burnup exceeding that typically reached by LEU fuel. The crack observed along most of the transverse cross-section of MNT-28W is believed to have originated from the alignment and interconnection of large porosity near the U-Mo/Zr interface. The interconnected large pores near the U-Mo/Zr interface are very likely where cracks can initiate and grow, and this behavior can be impacted by reactor shutdown stress. All the LALOs characterized in this study consisted of developed HBS with very few porous-free regions. The irradiated grain sizes were at least 20× less than the starting as-fabricated grain size. FGP interconnectivity was evident in all four LALO samples; however, FGP interconnection was more dramatic 5-15 µm away from the Zr diffusion barrier. Furthermore, with increasing distance from the 100µm-wide crack, there is a decrease in FGP size but not in porosity in the U-Mo fuel phase. Fission products, particularly Xe, penetrate the Zr diffusion barrier and are retained there in the first several microns of the diffusion barrier. The U-Mo/Zr interface becomes diffuse due to the penetration of Zr into the U-Mo fuel zone. An investigation of the creep behavior of the U-10Mo along the thickness and width of the fuel meat might provide more insight for fuel-swelling behavior and large-porosity formation.

# Acknowledgements

The funding for this work was provided by the U.S. Department of Energy, Office of Material Management and Minimization, National Nuclear Security Administration, under the Department of Energy-Office of Nuclear Energy (DOE-NE) Idaho Operations Office Contract DE-AC07-05ID14517. The authors would like to acknowledge the staff of the Irradiated Materials

Characterization Laboratory (IMCL) at the Materials and Fuels Complex (MFC) at Idaho National Laboratory for their effort in handling, preparation, and transfer of the specimens used in this work.

#### References

- [1] D. Keiser, J.F. Jue, B. Miller, J. Gan, A. Robinson, J. Madden, Observed Changes in As-Fabricated U-10Mo Monolithic Fuel Microstructures After Irradiation in the Advanced Test Reactor, Jom. 69 (2017) 2538–2545. https://doi.org/10.1007/s11837-017-2564-7.
- [2] D.E. Burkes, T. Hartmann, R. Prabhakaran, J.F. Jue, Microstructural characteristics of DU-xMo alloys with x = 7-12 wt%, J. Alloys Compd. 479 (2009) 140–147. https://doi.org/10.1016/j.jallcom.2008.12.063.
- [3] A.B. Robinson, G.S. Chang, D.D. Keiser Jr, D.M. Wachs, D.L. Porter, Irradiation Performance of U-Mo Alloy Based 'Monolithic'Plate-Type Fuel–Design Selection, INL Extern. Rep. INL/EXT-09-16807. (2009).
- [4] J. Gan, B.D. Miller, D.D. Keiser, J.F. Jue, J.W. Madden, A.B. Robinson, H. Ozaltun, G. Moore, M.K. Meyer, Irradiated microstructure of U-10Mo monolithic fuel plate at very high fission density, J. Nucl. Mater. 492 (2017) 195–203. https://doi.org/10.1016/j.jnucmat.2017.05.035.
- [5] J.F. Jue, D.D. Keiser, C.R. Breckenridge, G.A. Moore, M.K. Meyer, Microstructural characteristics of HIP-bonded monolithic nuclear fuels with a diffusion barrier, J. Nucl. Mater. 448 (2014) 250–258. https://doi.org/10.1016/j.jnucmat.2014.02.004.
- [6] K. Huang, Y. Park, D.D. Keiser, Y.H. Sohn, Interdiffusion between Zr diffusion barrier and U-Mo alloy, J. Phase Equilibria Diffus. 33 (2012) 443–449. https://doi.org/10.1007/s11669-012-0106-0.
- [7] Y. Park, D.D. Keiser, Y.H. Sohn, Interdiffusion and reactions between U-Mo and Zr at 650°C as a function of time, J. Nucl. Mater. 456 (2015) 351–358. https://doi.org/10.1016/j.jnucmat.2014.09.040.
- [8] F. Yan, X. Jian, S. Ding, Effects of UMo irradiation creep on the thermo-mechanical behavior in monolithic UMo/Al fuel plates, J. Nucl. Mater. 524 (2019) 209–217. https://doi.org/10.1016/j.jnucmat.2019.07.006.
- [9] D.D. Keiser, J.F. Jue, J. Gan, B.D. Miller, A.B. Robinson, J.W. Madden, M. Ross Finlay, G. Moore, P. Medvedev, M. Meyer, Microstructural characterization of an irradiated RERTR-6 U-7Mo/AA4043 alloy dispersion fuel plate specimen blister-tested to a final temperature of 500 °C, J. Nucl. Mater. 488 (2017) 100–122. https://doi.org/10.1016/j.jnucmat.2017.02.038.
- [10] J.M. Beeston, R.R. Hobbins, G.W. Gibson, W.C. Francis, Development and Irradiaton Performance of Uranium Aluminide Fuels in Test Reactors., Nucl. Technol. 49 (1980) 136–149. https://doi.org/10.13182/NT80-A32515.
- [11] D. Wachs, M. Meyer, Blister Threshold Based Thermal Limits for the U- Mo Monolithic

- Fuel System, in: Off. Sci. Tech. Inf. Tech. Reports, 2012.
- [12] P.G. Medvedev, H. Ozaltun, A.B. Robinson, B.H. Rabin, Shutdown-induced tensile stress in monolithic miniplates as a possible cause of plate pillowing at very high burnup, Nucl. Eng. Des. 328 (2018) 161–165. https://doi.org/10.1016/j.nucengdes.2018.01.004.
- [13] M.K. Meyer, J. Gan, J.F. Jue, D.D. Keiser, E. Perez, A. Robinson, D.M. Wachs, N. Woolstenhulme, G.L. Hofman, Y.S. Kim, Irradiation performance of U-Mo monolithic fuel, Nucl. Eng. Technol. 46 (2014) 169–182. https://doi.org/10.5516/NET.07.2014.706.
- [14] D.M. Perez, G.S. Chang, D.M. Wachs, N.E. Woolstenhulme, RERTR-12 Insertion 1 Irradiation Summary Report, 2012.
- [15] B.D. Miller, J. Gan, J. Madden, J.F. Jue, A. Robinson, D.D. Keiser, Advantages and disadvantages of using a focused ion beam to prepare TEM samples from irradiated U-10Mo monolithic nuclear fuel, J. Nucl. Mater. 424 (2012) 38–42. https://doi.org/10.1016/j.jnucmat.2012.01.022.
- [16] C.A. Smith, B.D. Miller, D. Keiser, A. Robinson, A. Aitkaliyeva, Microstructural response of the fuel phase in U-7Mo dispersion fuel irradiated at different powers, J. Nucl. Mater. 542 (2020) 152481. https://doi.org/10.1016/j.jnucmat.2020.152481.
- [17] C.A. Smith, D.D. Keiser, B.D. Miller, A. Aitkaliyeva, Microstructural dependence on fuel matrix composition in irradiated U-Mo dispersion fuels, J. Nucl. Mater. 550 (2021) 152943. https://doi.org/10.1016/j.jnucmat.2021.152943.
- [18] J.F. Jue, D.D. Keiser, B.D. Miller, J.W. Madden, A.B. Robinson, B.H. Rabin, Effects of irradiation on the interface between U-Mo and zirconium diffusion barrier, J. Nucl. Mater. 499 (2018) 567–581. https://doi.org/10.1016/j.jnucmat.2017.10.072.
- [19] C.A. Smith, S. Biswas, B.D. Miller, B. Kombaiah, D. Frazer, D.D. Keiser, A. Aitkaliyeva, High burnup structure formation in U-Mo fuels, J. Nucl. Mater. 563 (2022) 153617. https://doi.org/10.1016/j.jnucmat.2022.153617.
- [20] D. Jadernas, J. Gan, D. Keiser, J. Madden, M. Bachhav, J.-F. Jue, A. Robinson, Microstructural characterization of as-fabricated and irradiated U-Mo fuel using SEM/EBSD, J. Nucl. Mater. 509 (2018) 1–8. https://doi.org/10.1016/J.JNUCMAT.2018.06.007.
- [21] C.A. Smith, D.D. Keiser, B.D. Miller, A. Aitkaliyeva, Comparison of manual and automated image analysis techniques for characterization of fission gas pores in irradiated U-Mo fuels, Micron. 119 (2019) 98–108. https://doi.org/10.1016/j.micron.2019.01.008.